SCIENTIFIC REPORTS

OPEN

SUBJECT AREAS:
GENETICS
CELL BIOLOGY

Received
25 September 2014

Accepted
14 January 2015

Published
11 February 2015

Correspondence and requests for materials should be addressed to E.S.C. (bchces@nus.edu.sg)

Fitness Profiling Links Topoisomerase II Regulation of Centromeric Integrity to Doxorubicin Resistance in Fission Yeast

Thi Thuy Trang Nguyen[1,2], Julia Sze Lynn Lim[1,2], Richard Ming Yi Tang[1,2], Louxin Zhang[4,5] & Ee Sin Chen[1,2,3,4]

[1]Department of Biochemistry, National University of Singapore, Singapore 117597, [2]National University Health System (NUHS), Singapore, [3]Synthetic Biology Research Consortium, National University of Singapore, [4]NUS Graduate School for Integrative Sciences and Engineering, [5]Department of Mathematics, National University of Singapore, Singapore 119076.

Doxorubicin, a chemotherapeutic agent, inhibits the religation step of topoisomerase II (Top2). However, the downstream ramifications of this action are unknown. Here we performed epistasis analyses of *top2* with 63 genes representing doxorubicin resistance (DXR) genes in fission yeast and revealed a subset that synergistically collaborate with Top2 to confer DXR. Our findings show that the chromatin-regulating RSC and SAGA complexes act with Top2 in a cluster that is functionally distinct from the Ino80 complex. In various DXR mutants, doxorubicin hypersensitivity was unexpectedly suppressed by a concomitant *top2* mutation. Several DXR proteins showed centromeric localization, and their disruption resulted in centromeric defects and chromosome missegregation. An additional *top2* mutation could restore centromeric chromatin integrity, suggesting a counterbalance between Top2 and these DXR factors in conferring doxorubicin resistance. Overall, this molecular basis for mitotic catastrophe associated with doxorubicin treatment will help to facilitate drug combinatorial usage in doxorubicin-related chemotherapeutic regimens.

Doxorubicin is one of the most commonly used chemotherapeutic agents in the clinic and is a key component of major adjuvant regimens against solid tumours of the stomach, breast, urogenital, gynaecological and endocrine systems, as well as sarcomas, lymphomas and leukaemias[1]. The high efficacy of doxorubicin is connected to its rapid uptake by the cell, at a rate that much exceeds its rate of elimination[2,3]. Unfortunately, because of its high toxicity, profuse off-target effects, such as dose-dependent myelosuppression, cardiac, renal and liver toxicities, and even secondary leukaemia, are commonly associated with the use of the drug[2,4,5].

Doxorubicin consists of a planar ring structure that allows it to be readily intercalated into DNA helices—the primary target of the drug. Doxorubicin is generally believed to stabilize the cleavage complex of topoisomerase II and thereby prevent double-stranded DNA from being resealed[1,6]. This process eventually results in the formation of an overwhelming number of DNA double-stranded breaks (DSB) and the ensuing onset of apoptosis[4,6]. Doxorubicin has also been reported to disrupt mitochondrial membranes and cause the disassembly of the enzymatic chain that regulates oxidative phosphorylation. This, in turn, leads to the production of reactive oxygen species to destabilize cellular structures[5].

Recent studies also show that doxorubicin can disrupt chromatin in a Top2-independent manner by promoting histone eviction from the opened chromatin associated with the transcriptionally active genetic loci[7,8]. This activity of doxorubicin occurs independently from the induction of DSB and the concomitant eviction of histone γH2AX—a phosphorylated variant of histone H2A that is important for the coordination of DSB repair—thereby downplaying the DNA damage response and disrupting the repair of damaged chromatin. This mechanism can act synergistically with Top2 inhibition to enhance the cytotoxic effect of the drug. Another Top2 inhibitor, etoposide, does not show similar effects on histone exchange, indicating that this activity of doxorubicin is independent of Top2 catalytic inhibition[7,8]. Doxorubicin also disrupts gene transcription by regulating histone chaperone Asf1 protein levels during inhibition of DNA replication. It has been shown that degradation of Asf1 results in dechromatization of localized gene regions and in the firing of cryptic origins associated with regions that contain sequences without replication origins[9].

We previously performed a screen of 3225 single-gene knockout mutants and isolated 91 genes from *Schizosaccharomyces pombe* (fission yeast) underlying doxorubicin responsiveness. The identified genes include those that encode membrane-bound transporters, components of oxidative phosphorylation complexes residing on the inner membrane of the mitochondria, and numerous chromatin factors[10]. We further delineated the genetic relationship between these DXR genes and verified that they were, at least in part, present in human cells. This observation formed the basis with which to facilitate the isolation of a novel drug combination to sensitize human cancer cells to doxorubicin[11].

Because our initial screen could only test for genes that were non-essential for growth, fission yeast Top2 (*top2*$^+$) was not assessed. Here, we address the molecular implication of Top2 in the context of its interaction with DXR genes. We employed *top2-191*, a conditional mutant that contains a point mutation incorporated into the conserved DNA binding domain of fission yeast Top2 protein[12,13]. We performed tests at 26°C, at which the mutant is viable, and showed that Top2 acts synergistically with most of the DXR factors, including the network that probably functions to regulate DNA damage responses. Surprisingly, the doxorubicin hypersensitivity in several mutants, all of which showed a high degree of unequal chromosome segregation in the presence of the drug, was suppressed by the partial loss of Top2 function. These mutants resulted in a high level of non-coding transcripts that accompanies disruption to chromatin in the inner core of the centromere, which contains CENP-A. Consistently, similar disruptions to Top2 also suppressed the doxorubicin sensitivity of the fission yeast CENP-A mutant. These results suggest that doxorubicin disrupts centromeric chromatin but the epigenetic defect could be prevented by factors acting directly at the centromere to modulate CENP-A chromatin.

Results

Topoisomerase II is required for doxorubicin resistance in fission yeast. A chromatin epistasis group, comprising homologous recombination (HR) proteins, the SAGA histone acetyltransferase, and the chromatin remodelling Ino80 and RSC complexes, confers resistance against doxorubicin cytotoxicity in fission yeast cells[10]. Components of this epistasis group have been reported to control gene transcription and DNA repair, in which Top2 is also reported to play a role[14]. We sought to determine whether Top2 may cooperate in a similar functional group with these factors to counteract the cytotoxicity of doxorubicin in fission yeast.

We first constructed double mutants between the null alleles of 63 representative DXR genes of different ontological classification associated with doxorubicin resistance in fission yeast[10], with *top2-191* mutant. The *top2-191* mutant contains a point mutation in a highly conserved residue (A801V) in the DNA binding domain of fission yeast Top2 protein[12,15]. The temperature-sensitive *top2-191* mutant exhibited a prominent 'cut' (cell untimely torn) phenotype that was associated with chromosome condensation defects at the restrictive temperature (36°C)[13]. However, at the permissive temperature (26°C), *top2-191* exhibited a wild type (WT)-like phenotype, without detectable 'cut' cells (Supplementary Fig. 1)[13,16]. Interestingly, we observed that *top2-191* showed sensitivity to doxorubicin at 26°C, exhibiting 10-fold more sensitivity relative to the untreated control (Fig. 1A). WT cells did not show sensitivity over the 15–75 μg/ml doxorubicin concentration range (Fig. 1A). These observations suggested that the mitotic chromosome resolution defect of *top2-191* was physiologically distinct from the doxorubicin sensitivity phenotype. Another mutant *top2-342*, which contains G972D substitution also in the DNA binding domain[13], but at a non-conserved site, however did not exhibit sensitivity towards doxorubicin and hence was not chosen for further analyses (Supplementary Fig. 2).

Genetic interaction analyses of unique epistasis groups of DXR factors linked to Top2. We next interrogated the genetic relationship between DXR genes encoding the subunits of the SAGA, Ino80, and RSC complexes and proteins of the HR pathway with Top2 at 26°C (Fig. 1). This was achieved by comparing the drug hypersensitivity of double mutants of *top2-191* along with null mutants of *gcn5*, *ngg1* and *ada2* for the SAGA subunits, *iec1*, *SPCC16C4.20c* and *nht1* for the Ino80 components, *arp42*, *rsc1* and *rsc4* for the RSC subunits, and *rhp54* and *rhp55* for the HR proteins, with single mutants[10,17–20]. Two independent double mutant strains were constructed for each pair of single mutants to test the reproducibility of the observations. Ten-fold serially-diluted cultures of single and double mutants were spotted onto plates that contained various doxorubicin concentrations (15 to 75 μg/ml), and the synthetic growth defects observed for the double mutants relative to that of the single mutants were easily detectable over the lower concentration range of the drug.

Interestingly, we observed that *top2-191* showed a salient synthetic relationship with all mutants of the subunits of SAGA (Fig. 1A), Ino80 (Fig. 1B), and RSC (Fig. 1C) complexes and the HR proteins (Fig. 1D), indicating that Top2 was not epistatic to the SAGA-Ino80-RSC-HR network in regulating doxorubicin responsiveness[10]. Our genetic analyses further showed that *top2-191* showed a synergistic growth defect with the majority of the DXR mutants (Fig. 2, Supplementary Fig. 3–7). Specifically, these null mutations were in genes encoding components of the DASH complex (*dad2*, *dad3*, *dad5*, *duo1* and *spc19*) (Supplementary Fig. 3); the nucleotide synthesis pathway (*ada1*, *ccr4*, *csn1*, *csn2*, *SPAC2F3.11*) (Supplementary Fig. 4); mitochondrial function, particularly oxidative phosphorylation (*coq2*, *coq4*, *coq6*, *dps1*, *SPAC823.10c*, *SPBC1604.02c*, *SPBC947.14c*, *SPCC1672.04c*, *SPCC1840.09*, *tim11*) (Supplementary Fig. 5); intra- and extracellular trafficking (*apl6*, *npp106*, *pmd1*, *SPCC18.02*, *vph2*, *vps35*, *vps901*) (Supplementary Fig. 6); as well as chromatin- and non-chromatin-associated factors that modulate various nuclear processes (*git5*, *nrm1*, *rpa12*, *ssb3*, *SPAC31G5.19*, *SPAC4F10.04*, *SPBC21B10.13c/yox1*, *tup12*, *yaf9*) (Supplementary Fig. 7)[10]. Taken together, these results indicate that Top2 belongs to a unique functional group that is discrete from the bulk of the previously defined DXR network[10].

Modularity of the genetic interactions between Top2 and DXR gene. To better visualize the genetic interactions between *top2*$^+$ and DXR genes, we attempted to derive a descriptive matrix—a genetic interaction score (hereafter referred to as G.I. score)—to quantitate the severity of the hypersensitivity on plates across the varying drug concentrations. This G.I. score gives a measure of the mean growth retardation of the double mutants relative to that of parental single mutants on doxorubicin-incorporated plates (Supplementary Fig. 8A). We noted that some double mutants already exhibited slower growth on the plates in the absence of the drug, and this growth discrepancy was accounted for by normalizing the fitness scores of the double mutants on plates with and without the drug (Supplementary Fig. 8B). In this way, the G.I. score captures the genetic relationship described by growth that is solely dependent on the presence of doxorubicin (Supplementary Fig. 8B). The fitness values of the double mutants were assessed for each concentration of the drug. These values were then combined and logarithmically transformed to obtain the G.I. scores (Fig. 2A, Supplementary Fig. 8B). Thus, a G.I. score with a negative value for the mutant indicates a synergistic growth defect (SD) with *top2-191*; a positive value indicates a suppressive (SUP) relationship, in which the growth defect of a DXR mutant is suppressed by the introduction of *top2-191*; and a zero value indicates no cumulative synthetic growth defect (NSD) over that measured for the weaker of the parental single mutants (Supplementary Fig. 8C, D)[21].

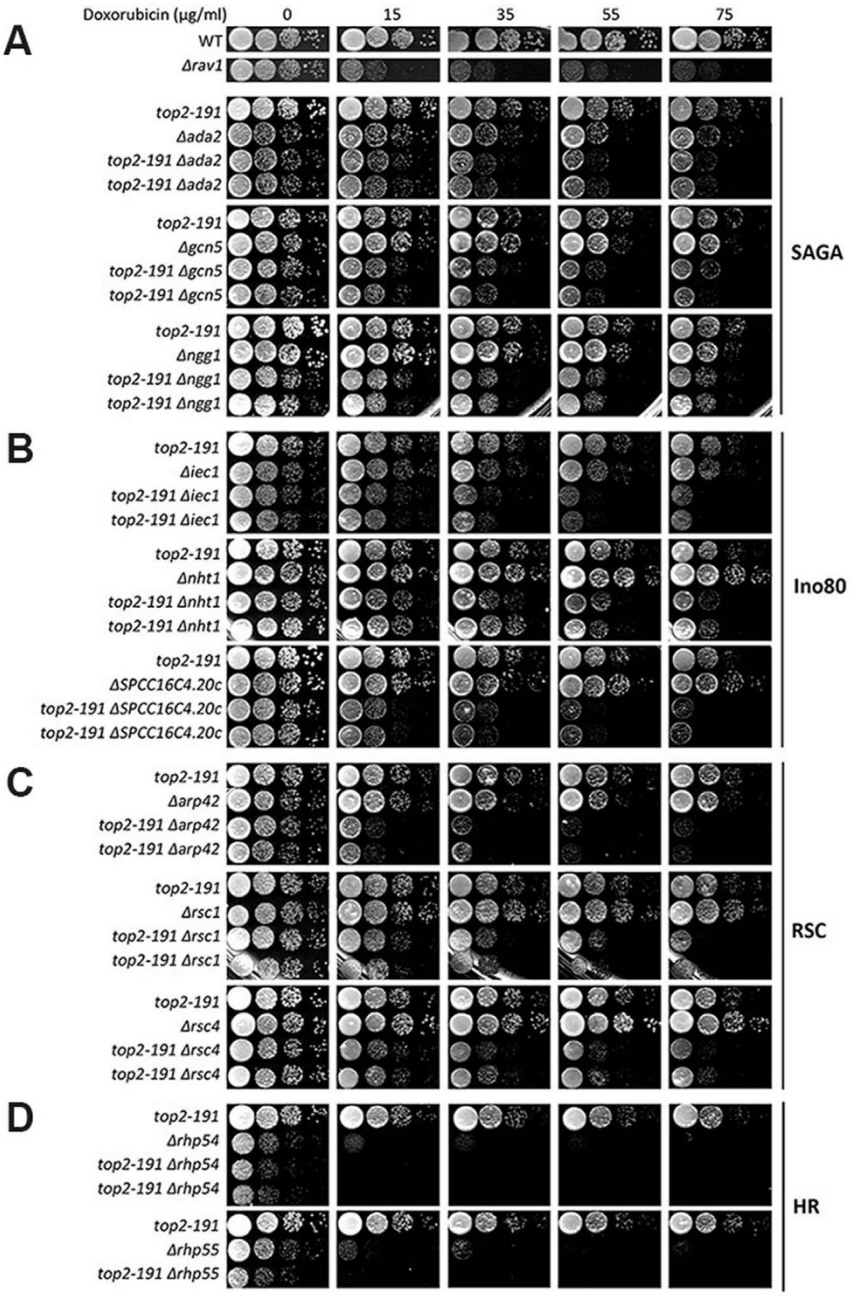

Figure 1 | Top2 functions synergistically with components of the doxorubicin resistance chromatin network. Doxorubicin hypersensitivity of the double mutants of *top2-191* with null mutants of (A) *ada2*, *ngg1* and *gcn5* (SAGA histone acetyltransferase complex); (B) *iec1*, *nht1*, *SPCC16C4.20c* (Ino80 chromatin remodelling complex); (C) *arp42*, *rsc1* and *rsc4* (RSC chromatin remodelling complex) and (D) *rhp54* and *rhp55* (homologous recombination factors). Cells were serially-diluted and spotted onto YEA media containing 0, 15, 35, 55 and 75 μg/ml doxorubicin. WT cells showed no drug sensitivity over this range of doxorubicin concentration. *Δrav1* was employed as the positive control. Two strains of double mutants were spotted for each gene pair to demonstrate data reproducibility.

The G.I. scores for all of the genetic interaction pairs studied in conjunction with *top2-191* were computed and subsequently consolidated, and then subjected to clustering analysis based on the Ward minimum variance clustering method (Fig. 2B, C)[22]. The mutants were clustered into one of five classes depicted as C-I to C-V and this is represented by differential colour-coding (Fig. 2B). Most of the DXR mutants showed a negative genetic interaction with *top2-191*, as indicated by growth on the plates with doxorubicin. We noticed several genes showing no and little cumulative upregulation in doxorubicin sensitivity when the respective null mutants were combined with *top2-191*, suggesting that these factors may act in the same complementation group as Top2. We also noticed that several mutants in C-I have standard deviations overlapping the NSD baseline (Fig. 2B, C). Under this criterion, *ΔSPBC19G7.10c*, *Δest1*, *ΔSPBC651.07*, *ΔSPAC2C4.05*, *Δcoq7* and *Δdph2* demonstrated no synthetic growth defect with *top2-191* (Fig. 2B-D, Fig. 3A). The remaining of C-I mutants possess low G.I. scores, indicating those mutants exhibited minimal synthetic growth defects with *top2-191*: *Δtim11, ΔSPBC947.14c, ΔSPAC11E3.12, ΔSPAC6G9.14, Δase1*, *Δdps1*, *Δsce3* and *Δrhp55* (Fig. 2B, C).

Of the characterized genes that belonged to the *top2* epistasis group, *coq7*$^+$ encodes a mono-oxygenase involved in coenzyme Q10 biosynthesis[23] and *est1*$^+$ transcribes a regulator of telomerase[24]. We have recently characterized *SPAC2C4.05* to encode a cornichon-

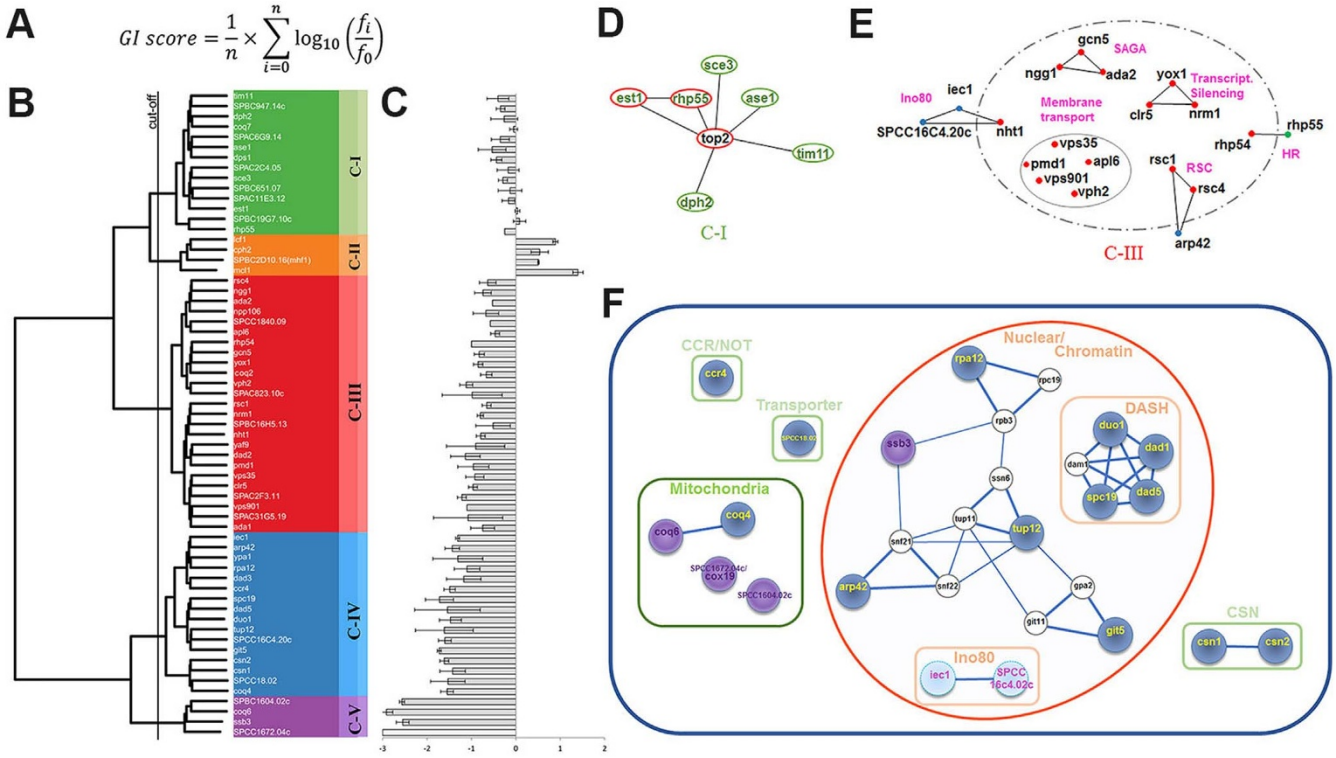

Figure 2 | Clustering analysis of epistasis relationship centred on Top2 using the G.I. scoring method to confer DXR in fission yeast. (A) Formula to calculate G.I. score. *f* is the relative fitness of the double mutant over that of the single mutant that showed weaker drug-dependent growth. f_i: fitness of the DXR mutant on drug-containing plate, f_0: fitness of the DXR strain on media with no drug, n: total number of concentrations of doxorubicin tested. (B) Ward minimum variance clustering of the DXR genes based on pairwise Euclidean distances between the corresponding vectors. Five classes (C-I to C-V) were differentiated base on the cut-off indicated at the position of the line. The five classes are differently colour-coded. (C) G.I. scores of the DXR mutants with respect to *top2-191*, corresponding to that in (B). (D) Functional association between the genes in C-I that belong to the similar epistasis group as Top2. Genes outlined in red have been shown to be linked to the telomeric chromatin regulation. (E) Functional grouping of C-III genes, which constituted the RSC and SAGA complexes. C-III also contains one member from the Ino80 (*nht1*) and HR (*rhp54*) functional group. Each circle corresponds to one gene and is colour-coded similar to (B): green: C-I, red: C-III and blue: C-IV. (F) Cellular compartment ontological categorization and functional network based on published links, as documented by String (version 9.1) to link C-IV (blue) and C-V (purple) genes. Interacting gene nodes that were revealed by String but not found in our DXR screen are denoted as white circles. C-V genes clustered as a mitochondrial group, whereas C-IV genes showed a preferential enrichment for nuclear chromatin into the DASH and Ino80 complexes as well as an extensive network likely to be regulating transcription.

like protein (Cor1) that modulates doxorubicin responsiveness in fission yeast with the Pmd1 transporter and vacuolar-ATPase[11]. Although the functional implications of the factors with *top2-191* in response to doxorubicin have yet to be clarified, there appears to exist more than one pathway involved in its function, as revealed through the functional protein association network (Fig. 2D), this network clustered *est1*$^+$ and *rhp55*$^+$ together, probably attributed to the link that both gene products, as well as Top2, have in maintaining the stability of telomere architecture[16,25]. The remaining four genes (*tim11*$^+$, *dph2*$^+$, *ase1*$^+$ and *sce3*$^+$), however, were functionally separated (Fig. 2B, C). These bioinformatics insights suggest that doxorubicin may result in the disruption of telomeric structure, mitochondrial membrane- and microtubule-related functions, the latter two deduced from the predicted connections of Tim11 as an inner mitochondrial ATPase subunit and Ase1 as an antiparallel microtubule crosslinking agent[10,26,27].

The mutated DXR genes that showed synthetic growth defects with *top2-191* were clustered into three major classes with an increasing trend of synthetic growth defect, as depicted by the negative G.I. scores (Fig. 2B, C; C-III (red), C-IV (blue) and C-V (purple) blocks). In the cluster C-III (red) (Fig. 2B), we noticed an enrichment of chromatin factors containing subunits of chromatin remodelling (*rsc1*, *rsc4*, *yaf9*), transcriptional silencing (*yox1*, *nrm1*, *clr5*), as well as modifiers regulating chromatin acetylation status (*gcn5*, *ada2*, *ngg1*)[18,19,28]. Mutants of the homologous recombination factor, *rhp54*, were also found in this class, as were majority of membrane-associated transporter mutants (*pmd1*, *vps35*, *vps901*, *apl6*, *vph2*), suggesting a close complementary relationship between intracellular transport factors and Top2 (Fig. 2E).

The mutants of chromatin remodelling Ino80 genes, *iec1* and *SPCC16C4.20c*, were clustered in class C-IV, separated from RSC and SAGA complex, and HR proteins, which were in class C-III (Fig. 2B, C). This dichotomy was surprising because we have previously attributed all four subgroups of proteins to the same complementation group[10]; this was, at that time, deduced from the lack of cumulative growth defects when the single mutants in each subgroup (RSC, Ino80, SAGA and HR) were combined with that from another. The new clustering method illuminated a potential role for Ino80 proteins in conjunction with Top2 to counteract doxorubicin cytotoxicity in a manner that is distinct from the other members of the complementation group (Fig. 2C).

Class C-IV genes were highly enriched in specific groups; in particular, the microtubule-kinetochore linking DASH complex and surprisingly, an extensive network that linked Rpa12, Tup12, Arp42, Git5 (C-IV, blue circles) to Ssb3 (C-V, purple circles) (Fig. 2F). These DXR genes were interconnected by several intermediary nodes (white circles), including several essential genes (*rph3*$^+$, *rpc19*$^+$, *snf21*$^+$)[29] that were not picked up in our initial

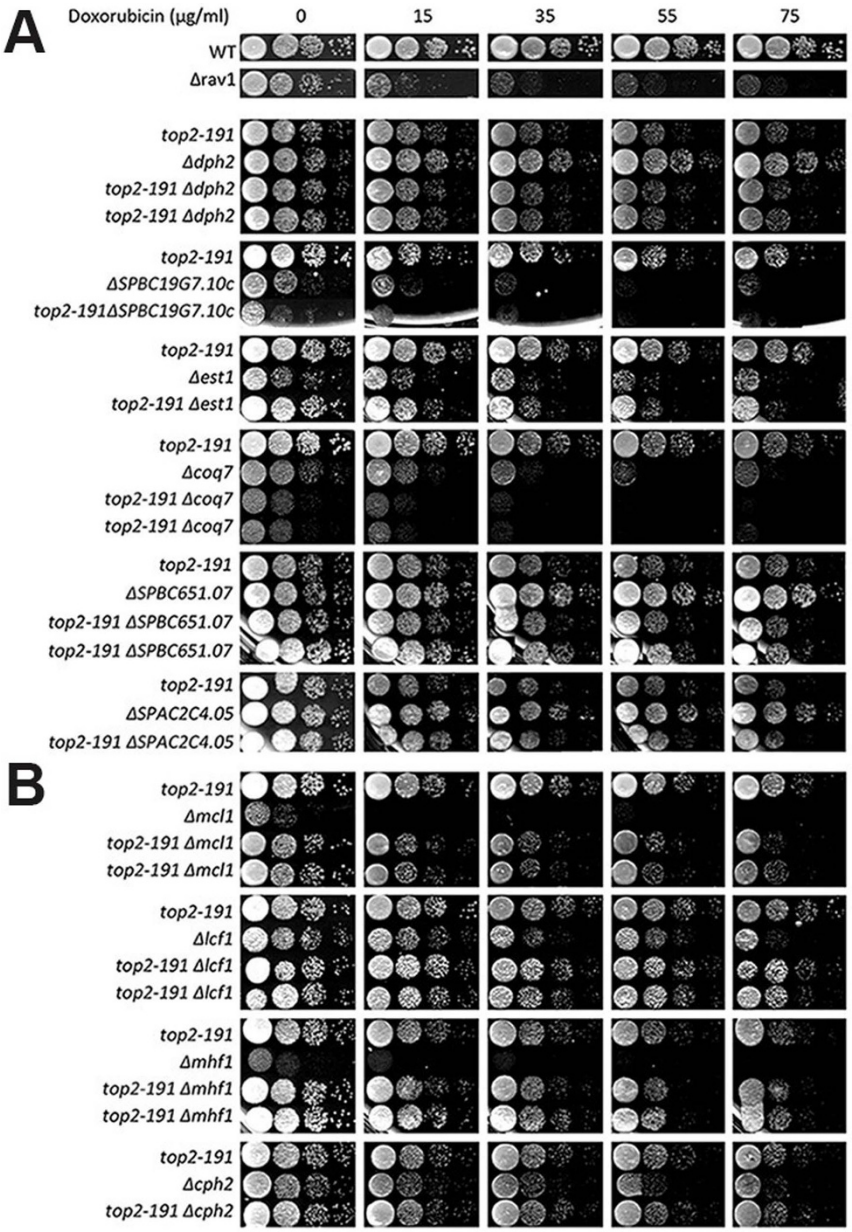

Figure 3 | Closely interacting DXR genes with the *top2-191* mutant. (A) DXR mutants (*Δdph2*, *ΔSPBC19G7.10c*, *Δest1*, *Δcoq7*, *ΔSPBC651.07*, and *ΔSPAC2C4.05*) that showed no cumulative growth defect when combined with *top2-191* compared to the growth of the single null mutant parents. *Δrav1* was employed as the positive control. (B) Positive genetic interaction where the growth defect of the *Δmcl1*, *Δmhf1*, *Δlcf1* and *Δcph2* in response to doxorubicin was suppressed by the concomitant introduction of *top2-191* mutation.

screen[10]. Besides *Δsnf22*, which was not tested in the screen, *Δtup11*, *Δssn6*, *Δgit11*, *Δgpa2* and *Δdam1* were tested but not picked up as positives[10]. Since the interaction data in the String database was obtained from strains without testing for drug effects (specifically doxorubicin), it is possible that there is a rewiring of the network with the drug, similar to that which occurs in response to DNA damaging stress[30].

Finally, most of the members of class C-V (*ΔSPBC1604.02c*, *Δcoq6* and *ΔSPBC1672.04c*/*cox19*; Fig. 2B, purple) were linked to mitochondrial functions, one of the three most important ontology groups previously reported to confer resistance against doxorubicin[10]. *Δssb3*, the null mutant of a single strand DNA-binding protein that functions in remediating S-phase DNA replication defects[31], was also clustered in this group of predominantly mitochondrial genes. It is possible that Ssb3 may function to maintain the stability of the mitochondrial genome (Fig. 2B, F).

Chromosome segregation defects in group class C-II DXR mutants is rescued by *top2* mutation. We were especially intrigued by class C-II mutants, (suppressive relationship with *top2-191*, positive G.I. scores) and the finding that doxorubicin hypersensitivity could be ameliorated by the introduction of *top2-191* (Fig. 2B, orange). Thus, from here, we sought to explore the molecular mechanism underlying the interaction of this SUP group of DXR factors with Top2. There were four mutants in this class of genes encoding Mcl1, Mhf1 (SPBC2D10.16), Lcf1 and Cph2 (Fig. 2B, C, 3B). Interestingly, several of these members have been reported to function at the fission yeast centromere: Mcl1, which is a regulator of DNA polymerase α, maintains the localization of the centromere-specific histone H3 variant CENP-A[32]. Mhf1, which forms part of the FANCM-MHF complex, was shown to be the counterpart of centromere binding protein CENP-S and also localizes to the centromere in fission yeast[33]. On the other hand Lcf1, a fatty acyl-CoA synthetase, and

Cph2, a subunit of the histone deacetylase complex have not been directly connected to centromeric function[34,35]. The reversion of the suppressive phenotype of two representative double mutants—*Δlcf1top2-191* and *Δmhf1top2-191*—to doxorubicin hypersensitivity via *top2*$^{+}$ overexpression, indicates that the SUP phenotype is directly linked to the disruption of *top2* function (Supplementary Fig. 9A, B).

In order to investigate the functional interaction of Top2 with Mcl1 and Mhf1, we thus studied the fidelity of chromosome segregation in the single and double mutants of *Δmcl1* and *Δmhf1* with *top2-191*, relative to that of WT cells. WT, single and double mutant cells were treated with 50 μg/ml doxorubicin for 4 h and were then assessed for changes in the nuclear morphology of the cells, particularly focusing on cells that showed defective execution of mitotic chromosomal segregation. The proportion of cells that showed defects were quantified among all binucleated mitotic and post-mitotic cells. We observed a prominent chromosome missegregation phenotype in *Δmcl1*: This resulted in (1) unequal partitioning of DNA leading to large and small nuclei on both ends of the cells, or (2) different numbers of nuclei at the two cell ends, which was often observed for cells unable to disjoin their chromosomes (Fig. 4A). Similar phenotypes have been described for mutants with defective centromeric chromatin[36–38].

After doxorubicin exposure for 4 h, *Δmcl1* cells demonstrated an approximately 10-fold increase in chromosome missegregation as compared with that of WT cells, constituting 28.93% of the total number of binucleated cells (28.3% unequal chromosome segregation with large and small nuclei; 0.6% non-disjunct segregation cells) (Fig. 4B). Surprisingly, the chromosome missegregation phenotype was strongly suppressed by the introduction of *top2-191* mutation, with the double mutant *Δmcl1top2-191* showing a decreased frequency of chromosome missegregation (13.38%; Fig. 4B). Comparatively, cells exhibiting chromosome missegregation constituted 40.74% of the total number of binucleated *Δmhf1* cells, which was more than 13-fold higher than that for WT counts. Doxorubicin-dependent chromosome missegregation could be suppressed in *Δmhf1* by *top2-191*; albeit, the effect was not as complete as that for *Δmcl1top2-191* at the same time point (Fig. 4C).

Top2 counteracts Mcl1 and Mhf1 in governing transcriptional repression at the inner centromeric core. The unequal chromosome segregation phenotype demonstrated by *Δmcl1* and *Δmhf1* was reminiscent of that exhibited by many mutants defective in the regulation of the chromatin integrity of the inner centromeric core, a site that determines bi-directionality of the chromosome segregation process[37]. Recently, it was found that disruptions to centromeric chromatin compaction can result in transcription of the underlying non-coding genomic DNA sequence[39]. To assess whether the *Δmcl1*- and *Δmhf1*-induced chromosome missegregation phenotype may be connected in this way, we attempted to detect the levels of the centromeric sequence-derived transcript using RT-PCR with centromere 1/3 specific primers. Consistent with the role of Mcl1 in maintaining the precise incorporation of the centromere-specific histone H3 variant CENP-A into the centromeric chromatin[32], a prominent level of transcript derived from the inner centromeric core sequence (*cnt1D*) was detected in the *Δmcl1* null mutant, interestingly, solely in the presence of doxorubicin (Fig. 5A, B). This transcript, however, was not detected in WT and *top2-191,* suggesting that the centromeric chromatin structure remained compact in these genetic backgrounds, with or without the drug. We were unable to detect a centromeric transcript when *top2-191* mutation was introduced into the *Δmcl1* background; this correlates well with the suppression of the chromosome segregation defect of *Δmcl1* by *top2-191* (Fig. 5A, B). We noted that this was not because of an effect on general

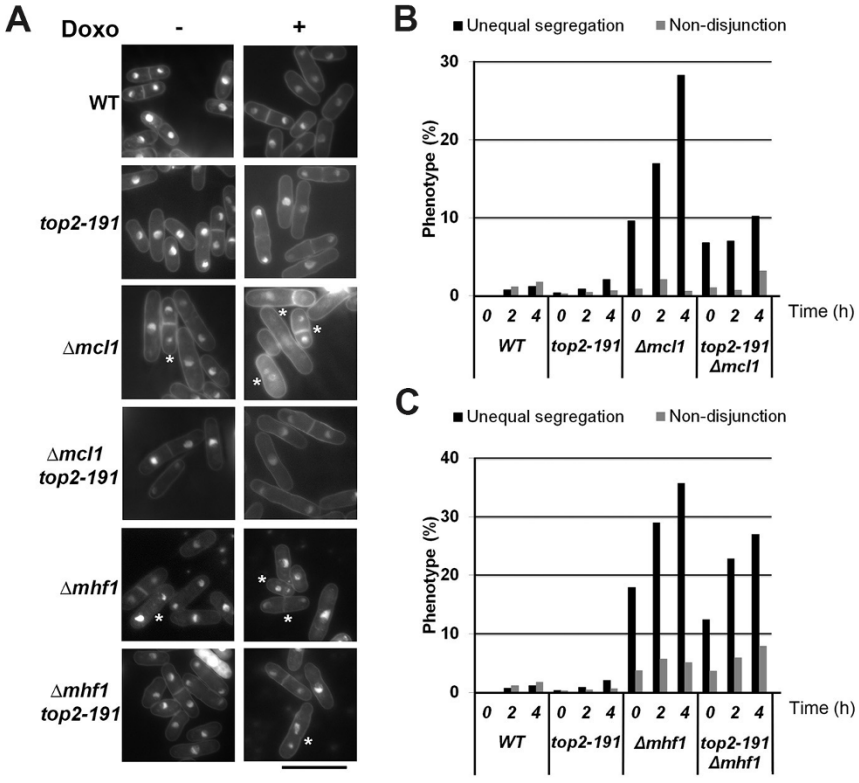

Figure 4 | (A) Chromosomal missegregation of *Δmcl1* and *Δmhf1* is suppressed by the *top2-191* mutation. White asterisks in (A) indicate cells exhibiting unequal chromosome segregation. (B–C) Proportion of multinucleated cells that showed unequal chromosome segregation (black) and non-disjunction (grey) of (B) WT, *top2-191*, *Δmcl1*, *Δmcl1top2-191* and (C) WT, *top2-191*, *Δmhf1*, *Δmhf1top2-191* mutants over the time course of 0, 2 and 4 h after 50 μg/ml doxorubicin was added to the cells.

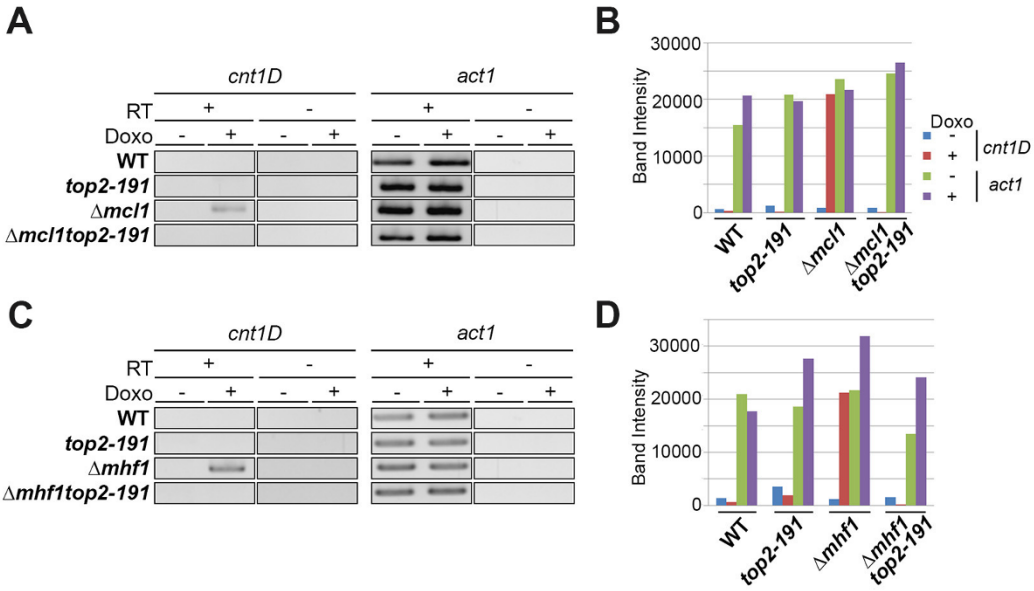

Figure 5 | Upregulation of centromeric DNA sequence derived-transcript in *Δmcl1* and *Δmhf1* was suppressed by the *top2-191* mutation. (A) Centromeric (*Cnt1D*) and actin (*act1*) transcripts were detected using RT-PCR in cells untreated (Doxo, -) or treated (Doxo, +) with 50 μg/ml doxorubicin. –RT represents no reverse transcription controls in WT, *top2-191*, *Δmcl1*, *Δmcl1top2-191* strains. (B) Quantitation of the *Cnt1D* and *act1* band intensity in (A). (C and D) The level of transcription of *Cnt1D* and *act1* under similar treatment conditions as in (A and B) in WT, *top2-191*, *Δmhf1*, *Δmhf1top2-191* strains. Result shown was obtained from one of two repeated experiments.

transcription, as similar transcript levels were detected for actin (*act1*) in WT, single and double mutants either treated or not with doxorubicin (Fig. 5A).

A similar trend was observed for *Δmhf1*, which showed an upregulation in centromeric sequence-derived transcript levels upon doxorubicin treatment, which could be suppressed in the *Δmhf1top2-191* double mutant (Fig. 5C, D). These results suggest that centromeric integrity was undermined by doxorubicin, but that Top2, Mcl1, and Mhf1 can interact to confer resistance against the genomic destabilization imposed by the drug.

Mcl1 acts upstream of CENP-A to determine the localization of the latter at the centromere[32]. It is likely that the synergistic effect of *Δmcl1* with doxorubicin may be connected to CENP-A; if so, then a loss-of-function mutation in CENP-A would be expected to also exhibit a similar genetic interaction with that of *top2*, as seen with *Δmcl1*. To test this, we combined a temperature sensitive CENP-A mutant, *cnp1-1*, with *top2-191*. *cnp1-1* contains an L87Q point mutation in the histone fold domain of the fission yeast CENP-A protein, which results in the mislocalization of CENP-A at a restrictive temperature[36]. We exposed *cnp1-1* on plates incorporated with doxorubicin at 26°C (permissive temperature for *cnp1-1* mutant) and observed a hypersensitivity of *cnp1-1* to doxorubicin. Interestingly, when *cnp1-1* was combined with *top2-191*, doxorubicin sensitivity was suppressed relative to that of the single mutant (Supplementary Fig. 10), as in the case of *Δmcl1top2-191*. Collectively, these results link doxorubicin sensitivity phenotype of *top2* with centromeric defects and represent a first important step towards elucidating the regulation of doxorubicin resistance by factors that maintain centromeric chromatin integrity.

Discussion

Topoisomerase II plays a central role in the activity of anthracycline compounds, which include doxorubicin[5,6]. A direct relationship is shown by the close association between the expression level of Top2 and the efficacy of doxorubicin in human cells[40]. In this study, we document the global epistatic relationship between Top2 in fission yeast and factors previously identified from a genome-wide chemogenomic study to regulate doxorubicin resistance[10]. This approach not only revealed that Top2 plays an essential role in safeguarding fission yeast cells against the cytotoxic effect of doxorubicin but also showed that Top2 probably forms a unique complementation group to govern genomic stability in the presence of the drug. We further showed that Top2 interacts closely with Mcl1 and Mhf1 to safeguard centromeric chromatin integrity, which, in turn, confers chromosome segregation fidelity in the cell cycle.

The allele-specificity in the doxorubicin hypersensitivity phenotype among different *top2* mutants may point to the differential importance of the amino acid residues in the three-dimensional structure of topoisomerase II with respect to its interaction with the drug. The crystal structure of the complex of human Top2β with DNA and another intercalating topoisomerase II inhibitor, etoposide, shows that the drug molecules are symmetrically lodged into base-pairs flanking the DNA cleavage sites. Doxorubicin, on the other hand, has been suggested to intercalate into DNA at approximately the same site on the Top2β molecule as that of etoposide albeit, technical challenges limited the confirmation of exact crystal structure[41]. In the case of etoposide, site directed mutagenesis studies revealed a critical stretch of residues ranging from glycine-465 (G465) to valine-925 (V925) on Top2β can control the potency of Top2 inhibitory drugs[15]. Sequence alignments show that fission yeast alanine-801 residue (A801), which is mutated in *top2-191* (A801V), is conserved with alanine-788 residue (A788) within this critical region of Top2β, whereas the mutated residue in fission yeast *top2-342* (G972D) is not conserved and corresponds to methionine-959 (M959) in Top2β (Supplementary Fig. 11)[13,15]. Top2β A788 is flanked by several functionally critical residues—glutamine-778 (Q778), arginine-820 (R820) and tyrosine-821 (Y821)—closely juxtaposing the drug interaction surface of Top2β[15]. Conversely, M959 is situated on the surface further away from the drug molecule-interacting pocket (Supplementary Fig. 12).

The spatial correlation thus suggests that the proximity of these mutated residues to the catalytic site of the SpTop2/HsTop2β determines doxorubicin hypersensitivity phenotype, probably due to the interruption of drug/DNA-interaction. Consistently, *top2-191* exhibited stronger attenuation of DNA relaxation activity compared with *top2-342*. While the activity was comparable with that of WT at

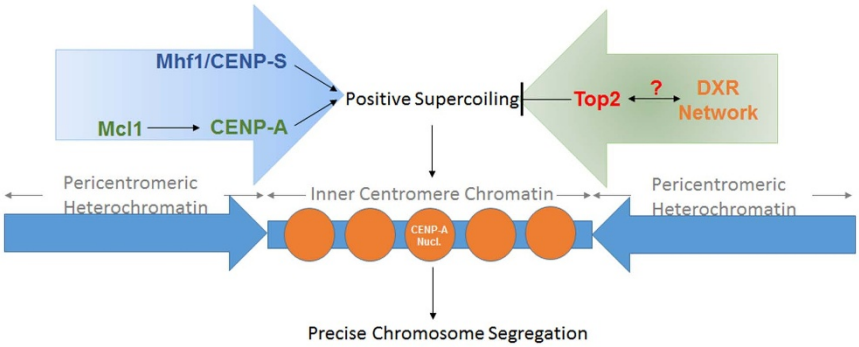

Figure 6 | Model to show the action of Top2 and CENP-A localized Mcl1 and Mhf1/CENP-S in counterbalancing the degree of positive supercoiling that determines chromatin integrity of the inner centromere. Top2 may synergize with some DXR genes to confer the release of positive supercoils. "?" indicates an unknown link(s).

permissive temperature (26°C), defect was apparent at semi-permissive temperatures (30°C) at which *top2-342* did not show much defect[42]. Furthermore, the rate of DNA relaxation of Top2 has been shown to be disrupted in *top2-191* mutant at permissive temperature to result in slower catalytic turnover[16], and thus it is possible that the prolonged accumulation of catalytic intermediates may serve to facilitate DNA intercalation of doxorubicin, which in turn, results in preferential killing of *top2-191* cells. At the current stage, our results cannot exclude the possibility that doxorubicin-sensitivity exhibited by *top2-191* may represent a gain-of-function phenotype, like that previously observed for suppression of cold sensitivity of the *Δtaz1* mutant linked to removal of telomeric entanglement during chromosome segregation[16].

The passage of DNA-processing machineries along the DNA fibre generates torsional stress on the topologically-constrained chromatin, and Top2 is essential for releasing such conformational stress by removing positive supercoils[14]. In many organisms, including fission yeast, Top2 also plays an important role in the resolution of sister chromatids during mitotic chromosome segregation. It has been shown in budding yeast that Top2 acts at the centromere to control the release of cohesin required for sister centromeres separation[43,44]. Top2 may be intentionally kept in check to permit catenation in order to synergize with cohesin and link sister centromeres together. This notion is consistent with the observation that disruption to Top2 function results in the suppression of premature centromere separation in mutated cohesin subunits[45,46]. It is thus possible that doxorubicin antagonism of centromeric chromatin integrity, leads to the precocious loss of cohesion between the sister centromeres and results in chromosome missegregation in DXR mutants. An untimely loss of sister centromeric cohesion may reduce tension on the spindle microtubule, which will cause spindle assembly checkpoint activation and in turn trigger a delay in metaphase and anaphase transitions[47]. However, we noted a lack of a high proportion of mitotic *Δmcl1* and *Δmhf1* cells exhibiting hypercondensed chromosomes—an indicator of metaphase arrest[48]—thus, suggesting the absence of a mitotic delay. Hence, this hypothesis is not likely to underlie the phenotype of class C-II mutants. Nevertheless, further experiments will be needed to ascertain the implication of cohesin regulation in doxorubicin resistance.

Very recently, Pang and colleagues showed that doxorubicin also promotes the rate of histone exchange, and is thus suggested to downregulate the DNA repair response through the removal of γH2AX[7]. It is possible that the intercalation of doxorubicin into the centromeric DNA may also disturb nucleosomal dynamics at the centromere. This would likely cause gross disruption to the centromeric chromatin, particularly when the ratio between histone H3 and the centromere-specific histone H3 variant CENP-A is strictly controlled[10]; shifting the equilibrium to incorporate more histone H3 would reduce cell viability[36,49]. The centromere-destabilization effect of doxorubicin would be expected to be even more pronounced upon the loss of the positive regulator of CENP-A localization. Another possibility is that higher order organization of centromeric chromatin may be maintained by DNA supercoiling, and that its disruption, such as with a *top2* mutation, may shift the equilibrium and thereby circumvent the need for factors such as Mcl1 and Mhf1 in the localization of the centromeric regulator, which would also include CENP-A (Fig. 6).

Extrapolating the results here to the regulation of chemoresistance in human cells, we predict that Top2 can improve doxorubicin efficacy by synergizing with loss of centromeric integrity. This hypothesis supports findings that doxorubicin-containing drug combinations and inhibitors of aurora kinases, which are essential in regulating CENP-A function[50], can result in improved therapeutic outcomes. In line with this hypothesis, several recent reports have shown synergism between doxorubicin and AT9283 and AS703569—kinase inhibitors of aurora A and B—in lung and breast cancer cells, respectively[51,52]. Our results further showed that disruption of Mcl1, a CENP-A localizing factor, sensitized fission yeast cells to doxorubicin via mitotic catastrophic chromosome segregation events. Although the mechanistic link between Top2 and CENP-A in doxorubicin efficacy has yet to be characterized in human cells, one study correlated reduced CENP-A levels to sensitization of hepatocellular carcinoma cells to doxorubicin[53].

Taken together, the findings reported here show a functional interaction between Top2 and factors that confer genomic stability at centromeric chromatin. This discovery is expected to fine-tune future development of new chemotherapeutic uses for doxorubicin in combination with other agents thereby reducing the side effects and improving drug efficacy.

Methods

Strains, culture conditions and genetic manipulation. Standard protocols for the manipulation of fission yeast were followed[54]. Prototrophic haploid fission yeast mutant strains with deletions of the DXR genes were previously reported[10]. These strains were constructed by crossing haploid gene knockout strains from ver1.0 and 2.0 libraries (Bioneer, Daejeon, Korea) with haploid WT fission yeast h^-972 strain, followed by random sporulation on Edinburgh Minimal Media (EMM) without amino acid supplement. The gene disruption in these mutants was verified by PCR using gene specific primers[10]. Temperature-sensitive *top2-191* strain[12] was obtained from Yeast Genetic Resource Center (Osaka, Japan). Construction of double mutants between the DXR mutants and *top2-191* strain was performed by crossing the respective strains at 26°C, followed by tetrad dissection using an MSM micromanipulator (Singer Instrument, Watchet, Somerset, UK). Thereafter, the *top2-191* mutation was selected for on the basis of temperature sensitivity at 36°C, linkage with *leu1* marker[42] and further confirmed by DNA sequencing. Doxorubicin (Wako Pure Chemical Industries, Osaka, Japan) treatment was performed at the indicated concentrations in YEA media (3% glucose, 0.5% yeast extract, 75 mg/ml adenine). Suppression of mutants by overexpression of $top2^+$ was performed by transforming empty REP81 vector and REP81-$top2^+$-FLAG (a gift from M. Yanagida) into yeast mutants and spotting the transformants onto doxorubicin-incorporated EMM-leucine plates.

Calculation of Genetic Interaction Score. The step-by-step derivation of the G.I. score is depicted in Supplementary Figure 8. Briefly, the growth fitness of the double mutant was obtained relative to that of the two parental single mutants that showed weaker growth on drug-incorporated plates separately (f_i). The fitness was also obtained for growth on plates not incorporated with doxorubicin (f_0). Relative growth fitness was obtained by f_i/f_0 ratio and a $\log_{10}$ transformation was imposed before the individual values were summed. Mean growth at each concentration was obtained by dividing by the number (n) of doxorubicin concentrations employed for the test. n = 4 in experiments described here (15, 35, 55, 75 μg/ml doxorubicin).

Statistical analyses. Experiments were repeated three times for the mean and standard deviation to be calculated using standard formula in Microsoft Excel 2013 (Redmond, WA). For clustering analysis, each gene corresponds to a four-dimensional vector (x1, x2, x3, x4), and xi is the mean value of the logarithm of the relative hypersensitivity of the corresponding double mutant at (20i-5) μg/ml for $1 \leq i \leq 4$. We computed all pairwise Euclidean distances between the corresponding vectors and then applied the Ward minimum variance clustering method[22], implemented in the R function *hclust*, to group the 63 genes.

Functional Protein Association Prediction. An online bioinformatics tool, String version 9.1, was employed to predict the functional connections between DXR protein groups[55]. Ontological pathways associated with the DXR genes were based on previous work[10].

Microscopy. All microscopic observations were performed on fission yeast cells at early-mid log growing phase, with the OD_{600} approximated to 0.5. Cells were fixed by 10% (final) glutaraldehyde (Sigma-Aldrich, St Louis, MO) on ice followed by three washes with ice cold 1×phosphate-buffered saline. Cells were mounted 1 : 1 with 4′, 6-diamidino-2-phenylindole (DAPI) (Life Technologies, Carlsbad, CA) before observation using a Nikon Ti-E inverted microscope (Nikon, Tokyo, Japan). More than 200 multinucleated cells were scored for chromosome segregation phenotype per sample.

DNA and RNA handling protocols. Genomic DNA was prepared by resuspending fission yeast cells in TE buffer (10 mM Tris-Cl pH 8.0, 2 mM EDTA) and vortexing with glassbeads in an equal volume of phenol/chloroform/isoamyl alcohol (24 : 23 : 1) (Nacalai, Kyoto, Japan) followed by ethanol precipitation of the aqueous phase. Genomic DNA was treated with 10 μg/ml RNase A (Roche, Basel, Switzerland) before further manipulation. Preparation of total RNA from fission yeast was previously reported[56]. Briefly, cells were disrupted with Trizol reagent (Nacalai, Kyoto, Japan) with glassbeads and RNA was ethanol precipitated from the aqueous phase. Five micrograms of total RNA was treated with DNase (Roche, Basel, Switzerland) and 100 ng of DNase-treated RNA was reverse transcribed and amplified (Onestep-RT kit, Qiagen, Limberg, Netherland)[56]. The non-reverse transcription (– RT) control was performed by immediately denaturing the reverse transcriptase at 95°C for 15 min upon addition of the reagent. Primers using for amplifying *act1* were 5′-GGCATCACACTTTCTACAACG-3′ and 5′-GAGTCCAAGACGATACCAGTG-3′; and *Cnt1D* were 5′-TTACGCTTCACCTAGTTTCC-3′ and 5′-ATTATTTTCCAGTATGCTGATG-3′. Gel band intensity obtained from electrophoresis was quantified by Image J software[57].

Viewing protein 3D structure. Protein 3D structure was analysed using Cn3D software[58].

1. Carvalho, F. S. *et al.* Doxorubicin-induced cardiotoxicity: from bioenergetics failure and cell death to cardiomyopathy. *Med. Res. Rev.* **34**, 106–135 (2014).
2. Tacar, O., Sriamornsak, P. & Dass, C. R. Doxorubicin: an update on anticancer molecular action, toxicity and novel drug delivery systems. *J. Pharm. Pharmacol.* **65**, 157–170 (2013).
3. Zheng, Z. *et al.* An ancestral haplotype defines susceptibility to doxorubicin nephropathy in the laboratory mouse. *J. Am. Soc. Nephrol.* **17**, 1796–1800 (2006).
4. Jamieson, D. & Boddy, A. V. Pharmacogenetics of genes across the doxorubicin pathway. *Expert Opin. Drug Metab. Toxicol.* **7**, 1201–1210 (2011).
5. Carvalho, C. *et al.* Doxorubicin: the good, the bad and the ugly effect. *Curr. Med. Chem.* **16**, 3267–3285 (2009).
6. Pommier, Y., Leo, E., Zhang, H. & Marchand, C. DNA topoisomerases and their poisoning by anticancer and antibacterial drugs. *Chem. Biol.* **17**, 421–433 (2010).
7. Pang, B. *et al.* Drug-induced histone eviction from open chromatin contributes to the chemotherapeutic effects of doxorubicin. *Nat. Commun.* **4**, 1908 (2013).
8. Yang, F., Kemp, C. J. & Henikoff, S. Doxorubicin enhances nucleosome turnover around promoters. *Curr. Biol.* **23**, 782–787 (2013).
9. Im, J. S. *et al.* ATR checkpoint kinase and CRL1βTRCP collaborate to degrade ASF1a and thus repress genes overlapping with clusters of stalled replication forks. *Genes Dev.* **28**, 875–887 (2014).
10. Tay, Z. *et al.* Cellular robustness conferred by genetic crosstalk underlies resistance against chemotherapeutic drug doxorubicin in fission yeast. *PLoS One* **8**, e55041 (2013).
11. Tay, Z. *et al.* P-glycoprotein and vacuolar ATPase synergistically confer anthracycline resistance to fission yeast and human cells. *Curr. Med. Chem.* **21**, 251–260 (2014).
12. Shiozaki, K. & Yanagida, M. A. Functional 125-kDa core polypeptide of fission yeast DNA topoisomerase II. *Mol. Cell. Biol.* **11**, 6093–6102 (1991).
13. Nakazawa, N., Mehrotra, R., Ebe, M. & Yanagida, M. Condensin phosphorylated by the aurora-like kinase Ark1 is continuously required until telophase in a mode distinct from Top2. *J. Cell Sci.* **124**, 1795–1807 (2011).
14. Wang, J. C. Cellular roles of DNA topoisomerases: a molecular perspective. *Nat. Rev. Mol. Cell Biol.* **3**, 430–440 (2002).
15. Wu, C. C. *et al.* Structural basis of type II topoisomerase inhibition by the anticancer drug etoposide. *Science* **333**, 459–462 (2011).
16. Germe, T., Miller, K. & Cooper, J. P. A non-canonical function of topoisomerase II in disentangling dysfunctional telomeres. *EMBO J.* **28**, 2803–2811 (2009).
17. Hogan, C. J. *et al.* Fission yeast Iec1-Ino80-mediated nucleosome eviction regulates nucleotide and phosphate metabolism. *Mol. Cell. Biol.* **30**, 657–674 (2010).
18. Helmlinger, D. *et al.* The *S. pombe* SAGA complex controls the switch from proliferation to sexual differentiation through the opposing roles of its subunits Gcn5 and Spt8. *Genes Dev.* **22**, 3184–3195 (2008).
19. Monahan, B. J. *et al.* Fission yeast SWI/SNF and RSC complexes show compositional and functional differences from budding yeast. *Nat. Struct. Mol. Biol.* **15**, 873–880 (2008).
20. Khasanov, F. K. *et al.* A new recombinational DNA repair gene from *Schizosaccharomyces pombe* with homology to Escherichia coli Rec A. *Genetics* **152**, 1557–1572 (1999).
21. Dixon, S. J. *et al.* Systematic mapping of genetic interaction networks. *Annu. Rev. Genet.* **43**, 601–625 (2009).
22. Ward Jr, J. H. Hierarchical grouping to optimize an objective function. *J. Am. Stat. Assoc.* **58**, 236–244 (1963).
23. Miki, R., Saiki, R., Ozoe, Y. & Kawamukai, M. Comparison of a coq7 deletion mutant with other respiration-defective mutants in fission yeast. *FEBS J.* **275**, 5309–5324 (2008).
24. Beernink, H. T. *et al.* Telomere maintenance in fission yeast requires an Est1 ortholog. *Curr. Biol.* **13**, 575–580 (2003).
25. Cullen, J. K. *et al.* Break-induced loss of heterozygosity in fission yeast: dual roles for homologous recombination in promoting translocations and preventing de novo telomere addition. *Mol. Cell Biol.* **27**, 7745–7757 (2007).
26. Yamashita, A. *et al.* The roles of fission yeast Ase1 in mitotic cell division, meiotic nuclear oscillation, and cytokinesis checkpoint signaling. *Mol. Biol. Cell* **16**, 1378–1395 (2005).
27. Tokatlidis, K. *et al.* Translocation arrest of an intramitochondrial sorting signal next to Tim11 at the inner-membrane import site. *Nature* **384**, 585–588 (1996).
28. Caetano, C., Klier, S. & de Bruin, R. A. Phosphorylation of the MBF repressor Yox1 by the DNA replication checkpoint keeps the G1/S cell-cycle transcriptional program active. *PLoS One* **6**, e17211 (2011).
29. Kim, D. U. *et al.* Analysis of a genome-wide set of gene deletions in the fission yeast *Schizosaccharomyces pombe*. *Nat. Biotechnol.* **28**, 617–623 (2010).
30. Bandyopadhyay, S. *et al.* Rewiring of genetic networks in response to DNA damage. *Science* **330**, 1385–1389 (2010).
31. Cavero, S., Limbo, O. & Russell, P. Critical functions of Rpa3/Ssb3 in S-phase DNA damage responses in fission yeast. *PLoS Genet.* **6**, e1001138 (2010).
32. Natsume, T. *et al.* A DNA polymerase alpha accessory protein, Mcl1, is required for propagation of centromere structures in fission yeast. *PLoS One* **3**, e2221 (2008).
33. Bhattacharjee, S. *et al.* MHF1-2/CENP-S-X performs distinct roles in centromere metabolism and genetic recombination. *Open Biol.* **3**, 130102 (2013).
34. Oshiro, T., Aiba, H. & Mizuno, T. A defect in a fatty acyl-CoA synthetase gene, lcf1+, results in a decrease in viability after entry into the stationary phase in fission yeast. *Mol. Gen. Genomics* **269**, 437–442 (2003).
35. Nicolas, E. *et al.* Distinct roles of HDAC complexes in promoter silencing, antisense suppression and DNA damage protection. *Nat. Struct. Mol. Biol.* **14**, 372–380 (2007).
36. Chen, E. S., Saitoh, S., Yanagida, M. & Takahashi, K. A cell cycle-regulated GATA factor promotes centromeric localization of CENP-A in fission yeast. *Mol. Cell* **11**, 175–187 (2003).
37. Takahashi, K., Chen, E. S. & Yanagida, M. Requirement of Mis6 centromere connector for localizing a CENP-A-like protein in fission yeast. *Science* **288**, 2215–2219 (2000).
38. Ohkura, H. *et al.* Cold-sensitive and caffeine-supersensitive mutants of the *Schizosaccharomyces pombe dis* genes implicated in sister chromatid separation during mitosis. *EMBO J.* **7**, 1465–1473 (1988).
39. Choi, E. S. *et al.* Identification of noncoding transcripts from within CENP-A chromatin at fission yeast centromeres. *J. Biol. Chem.* **286**, 23600–23607 (2011).
40. Burgess, D. J. *et al.* Topoisomerase levels determine chemotherapy response in vitro and in vivo. *Proc. Natl. Acad. Sci. U S A* **105**, 9053–9058 (2008).
41. Wu, C. C. *et al.* On the structural basis and design guidelines for type II topoisomerase-targeting anticancer drugs. *Nucleic Acids Res.* **41**, 10630–10640 (2013).
42. Uemura, T. & Yanagida, M. Isolation of type I and II DNA topoisomerase mutants from fission yeast: single and double mutants show different phenotypes in cell growth and chromatin organization. *EMBO J.* **3**, 1737–1744 (1984).
43. Gómez, R. *et al.* Cohesin removal precedes topoisomerase IIα-dependent decatenation at centromeres in male mammalian meiosis II. *Chromosoma* **123**, 129–146 (2014).

44. Bachant, J. *et al.* The SUMO-1 isopeptidase Smt4 is linked to centromeric cohesion through SUMO-1 modification of DNA topoisomerase II. *Mol. Cell* **9**, 1169–1182 (2002).
45. Toyoda, Y. & Yanagida, M. Coordinated requirements of human topo II and cohesion for metaphase centromere alignment under Mad2-dependent spindle checkpoint surveillance. *Mol. Biol. Cell* **17**, 2287–2302 (2006).
46. Díaz-Martínez, L. A., Giménez-Abián, J. F. & Clarke, D. J. Chromosome cohesion - rings, knots, orcs and fellowship. *J. Cell Sci.* **121**, 2107–2114 (2008).
47. Hoque, M. T. & Ishikawa, F. Cohesin defects lead to premature sister chromatid separation, kinetochore dysfunction, and spindle-assembly checkpoint activation. *J. Biol. Chem.* **277**, 42306–42314 (2002).
48. Hiraoka, Y., Toda, T. & Yanagida, M. The NDA3 gene of fission yeast encodes beta-tubulin: a cold-sensitive nda3 mutation reversibly blocks spindle formation and chromosome movement in mitosis. *Cell* **39**, 349–358 (1984).
49. Castillo, A. G. *et al.* Plasticity of fission yeast CENP-A chromatin driven by relative levels of histone H3 and H4. *PLoS Genet.* **3**, e121 (2007).
50. Kunitoku, N. *et al.* CENP-A phosphorylation by Aurora-A in prophase is required for enrichment of Aurora-B at inner centromeres and for kinetochore function. *Dev. Cell* **5**, 853–864 (2003).
51. Jayanthan, A. *et al.* Occurrence and modulation of therapeutic targets of aurora kinase inhibition in pediatric acute leukemias cells. *Leuk. Lymphoma* **54**, 1505–1516 (2013).
52. Romanelli, A. *et al.* Inhibiting aurora kinases reduces tumor growth and suppresses tumor recurrence after chemotherapy in patient-derived triple-negative breast cancer xenografts. *Mol. Cancer Ther.* **11**, 2693–2703 (2012).
53. Eom, Y. W. *et al.* Two distinct modes of cell death induced by doxorubicin: apoptosis and cell death through mitotic catastrophe accompanied by senescence-like phenotype. *Oncogene* **24**, 4765–4777 (2005).
54. Moreno, S., Klar, A. & Nurse, P. Molecular genetic analysis of fission yeast *Schizosaccharomyces pombe*. *Methods Enzymol.* **194**, 795–823 (1991).
55. Franceschini, A. *et al.* STRING v9.1: protein-protein interaction networks, with increased coverage and integration. *Nucleic Acids Res.* **41**, D808–D815 (2013).
56. Chen, E. S. *et al.* Cell cycle control of centromeric repeat transcription and heterochromatin assembly. *Nature* **451**, 734–737 (2008).
57. Schneider, C. A., Rasband, W. S. & Eliceiri, K. W. NIH Image to ImageJ: 25 years of image analysis. *Nat. Methods* **9**, 671–675 (2012).
58. Madej, T. *et al.* MMDB: 3D structures and macromolecular interactions. *Nucleic Acids Res.* **40**, D461–D464 (2012).

Acknowledgments

We thank Yeast Genetic Resource Center (YGRC) for strains, Huifang Guo, Yue Rong Tan and Siew Lee Chan for technical support, Dechao Tian for help with clustering algorithm, Dr. Kenneth Ban and the members of Chen lab for discussion. We are very grateful to Mitsuhiro Yanagida for *top2-342* strains and *top2*$^{+}$ overexpression plasmid. We thank Rebecca Anne Jackson for critically editing the manuscript. This work is supported by a Singapore Ministry of Education Tier II grant (MOE2010-T2-1-111) awarded to ESC. TTTN was a recipient of the scholarship to foreign undergraduate student awarded by Singapore Ministry of Education.

Author contributions

T.T.T.N. and J.S.L.L. performed all experiments, T.T.T.N., R.M.Y.T. and L.Z. derived the G.I. score calculation method, L.Z. performed clustering analyses, E.S.C. conceived the project, obtained grant funding, coordinated the project and wrote the manuscript.

Additional information

Supplementary information accompanies this paper at http://www.nature.com/scientificreports

Competing financial interests: The authors declare no competing financial interests.

How to cite this article: Nguyen, T.T.T., Lim, J.S.L., Tang, R.M.Y., Zhang, L. & Chen, E.S. Fitness Profiling Links Topoisomerase II Regulation of Centromeric Integrity to Doxorubicin Resistance in Fission Yeast. *Sci. Rep.* **5**, 8400; DOI:10.1038/srep08400 (2015).